

Nanoscale phase behavior on flat and curved membranes

This content has been downloaded from IOPscience. Please scroll down to see the full text.

2014 Nanotechnology 25 505101

(<http://iopscience.iop.org/0957-4484/25/50/505101>)

View [the table of contents for this issue](#), or go to the [journal homepage](#) for more

Download details:

IP Address: 130.225.121.138

This content was downloaded on 02/12/2014 at 09:50

Please note that [terms and conditions apply](#).

Nanoscale phase behavior on flat and curved membranes

Thomas Andersen¹, Azra Bahadori¹, Dino Ott¹, Anders Kyrsting¹,
S Nader S Reihani^{1,2} and Poul M Bendix¹

¹Niels Bohr Institute, University of Copenhagen, Blegdamsvej 17, DK-2100 Copenhagen, Denmark

²Department of Physics, Sharif University of Technology, Teheran 11365-9161, Iran

E-mail: bendix@nbi.dk

Received 15 August 2014, revised 21 October 2014

Accepted for publication 30 October 2014

Published 28 November 2014

Abstract

The diverse physical properties of membranes play a critical role in many membrane associated biological processes. Proteins responsible for membrane transport can be affected by the lateral membrane order and lateral segregation of proteins is often controlled by the preference of certain membrane anchors for membrane phases having a physically ordered state. The dynamic properties of coexisting membrane phases are often studied by investigating their thermal behavior. Optical trapping of gold nanoparticles is a useful tool to generate local phase transitions in membranes. The high local temperatures surrounding an irradiated gold nanoparticle can be used to melt a part of a giant unilamellar lipid vesicle (GUV) which is then imaged using phase sensitive fluorophores embedded within the bilayer. By local melting of GUVs we reveal how a protein-free, one component lipid bilayer can mediate passive transport of fluorescent molecules by localized and transient pore formation. Also, we show how tubular membrane curvatures can be generated by optical pulling from the melted region on the GUV. This will allow us to measure the effect of membrane curvature on the phase transition temperature.

 Online supplementary data available from stacks.iop.org/NANO/25/505101/mmedia

Keywords: nanoscale phase behavior, membrane curvature, membrane permeability, optical trapping, local phase transitions, optical heating, lipid tubes

(Some figures may appear in colour only in the online journal)

1. Introduction

Plasmonic heating resulting from irradiation of metal nanoparticles using resonant light has become a useful tool for localized thermal induction of heat in biological materials. There are huge prospects for this technique in photothermal therapy [1], but also for investigation of thermal effects at the molecular level on specific heat sensing proteins [2] or the exploration of local heat effects on membranes [3, 4]. The thermal properties of membranes have been studied for decades and only recently has it become possible to experimentally probe the thermal response of a membrane to a local heat gradient using optical trapping of metal nanoparticles as heat probes [3–6]. Such an experimental assay provides a tool to investigate recent theoretical predictions regarding the

behavior of biological systems existing within temperature gradients [7].

Membrane permeability is well known to be enhanced during the main melting transition of lipid bilayers [8–10]. However, little is known about the nature and mechanism of this leakage. Measurements have so far been performed using electrical conductance measurements across flat black lipid membranes (BLMs) [11, 12]. BLMs can contain remnants of organic solvents used in the formation process which can potentially influence the results. Fluorescence permeability measurements have so far not confirmed the discrete events detected in electrical BLM measurements. One reason for this could be that transient fluorescent signals from permeability measurements are difficult to detect due to the rapid diffusion and consequent dilution of dyes.

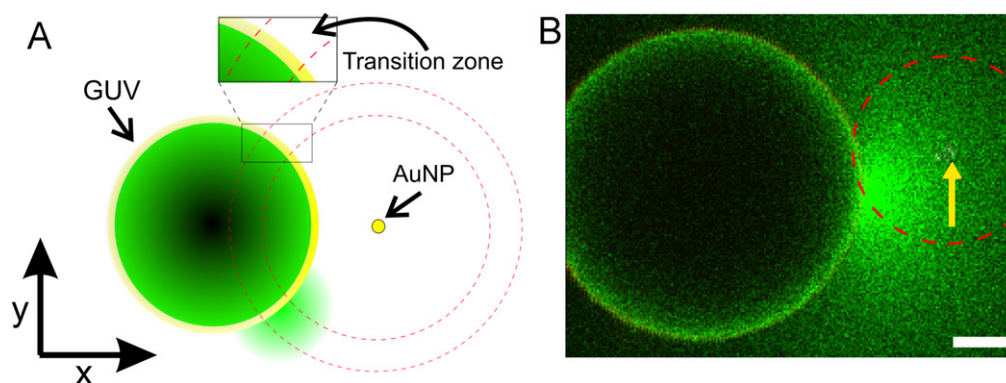


Figure 1. Setting up coexisting fluid and gel phases on a single GUV for studying membrane permeability. (A) Schematic depiction of an optically trapped $d=80$ nm AuNP close to a GUV made from DC₁₅PC which is gently adhered to a passivated glass surface. The GUV has a phase transition temperature of $T_m=33$ °C. The region within the annular ring corresponds to the membrane area that exists within the transition region ($\Delta T \sim 1$ °C). The GUV stays in gel phase further away whereas the proximal part of the GUV is fluid. A leakage of calcein dye (green hazy disk) is depicted centered on the surface of the GUV. (B) Data showing detection of a leakage event. During leakage the calcein dilutes and de-quenches to yield a powerful burst in intensity. The red dashed circle marks a melting distance within the annular ring also depicted in (A). The scale bar is $5 \mu\text{m}$.

Here we show how membrane permeability can be measured using fluorescence in conjunction with localized heating of GUVs using an optically trapped gold nanoparticle (AuNP). The fluorescent assay includes self-quenched calcein within the GUVs which dequenches during permeation across the GUV membrane and consequently gives a powerful burst in intensity that lasts up to a few seconds depending on the life-time of the pore event [4]. By using membrane incorporated phase sensitive dyes we can clearly visualize the melted region and confirm that melting actually takes place within the membrane.

We demonstrate the versatility of this assay and show how membrane tubes can be pulled from the fluid part of the membrane by combining optical heating with optical pulling in a dual trap system. This assay will provide the possibility to regulate the curvature and membrane phase within the same GUV and hence the effect of curvature on the membrane phase transition temperature can be investigated. Finally, we show how a local liquid disordered phase can be established on a tube pulled from a GUV existing in a liquid ordered phase, thus creating phase domain interfaces on a highly curved bilayer without fissioning of the tube.

2. Results

2.1. Localized melting of GUVs

Giant unilamellar lipid vesicles (GUVs) composed of DC₁₅PC ($T_m=33$ °C) were locally heated using optically trapped AuNPs with a diameter of 80 nm. By changing the distance between the GUV and the nanoparticle, a transition zone was established on the GUV which allowed us to study permeability, as shown in figure 1.

As a reporter for permeability changes and phase changes within the GUV membrane we use the aqueous dye calcein and two different phase sensitive fluorescent markers: laurdan and di-4-ANEPPDHQ, respectively. Calcein, which was used

for detecting bilayer permeation, was encapsulated at self-quenched concentrations (up to 80 mM) but with significant variability in the encapsulation efficiency among the different GUVs. A typical image of the variability in encapsulation efficiency is shown in figure 2(A). GUVs containing calcein at self-quenched concentrations have a characteristic dark center region surrounded by a brighter peripheral region. The dark regions are caused by attenuation of excitation light due to absorption as it travels through the lumen of the GUV containing high concentrations of absorbing calcein. This effect is less pronounced at the peripheral regions due to the curvature of the GUVs.

To visualize the fluid region of a gel phase GUV we used the potentiometric dye, di-4-ANEPPDHQ, which incorporates predominantly into more disordered domains of GUVs [4, 13], as shown in figure 2(B). We did not measure a significant incorporation of the dye into the gel phase but found that the fluorophore incorporated directly from solution into the disordered fluid phase.

Lipid bilayers exhibit radically different hydration levels in gel and fluid phases [15]. To verify that the locally heated region as shown in figure 2(B) is in fact in fluid phase we measured the degree of hydration using laurdan which senses the hydration level of the bilayer. Laurdan exhibits a 50 nm spectral red shift in non-polar versus polar environments [15]. Since laurdan does not exhibit lateral partitioning it is possible to measure the spectral shift by quantifying the relative intensities from the spectral regions defined as: $I_{420-460}$ (I_B) and $I_{461-530}$ (I_R) respectively. In gel phase laurdan will predominantly emit in the region from 420–460 nm whereas in fluid phase the laurdan emission will red shift leading to an increased intensity in the wavelength interval 461–530 nm. This can be expressed as a single parameter called the generalized polarization G_p

$$G_p = \frac{I_B - I_R}{I_B + I_R}. \quad (1)$$

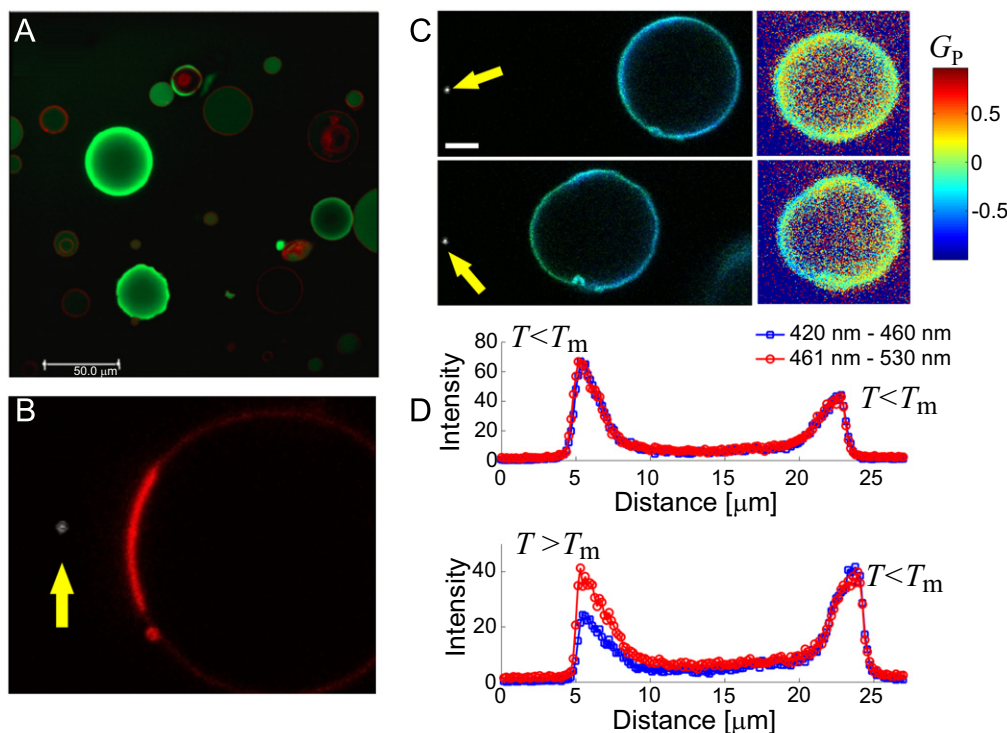


Figure 2. Fluorescent markers used for detecting permeability and co-existing phases originating from local heating. (A) Encapsulation of calcein within GUVs at self-quenching concentrations (maximum concentration, $c = 80$ mM). A dark region surrounded by a bright intensity indicates a high degree of self-quenching. GUVs containing variable concentrations of calcein, as well as multilamellar vesicles and lipid-aggregates are seen in the sample chamber. GUVs are labeled with the red membrane dye TR-DHPE. (B) Clear visualization of the extent of the fluid phase using di-4-ANEPPDHQ (red color) which strongly partitions into the fluid phase. (C) The environmentally sensitive fluorescent dye laurdan reveals the level of hydration within the bilayer. Top images show a GUV in gel phase at $T \sim 25$ °C (scale bar is $5 \mu\text{m}$). Bottom images show a GUV which is locally melted. The top and bottom right images show a plot of the G_p values based on equation (3). The melted region has lower G_p values than the region which is still in gel phase thus revealing the increased level of hydration which is a signature of the fluid phase. (D) A line scan across the GUV at $T \sim 25$ °C (upper figure) and after local melting of the GUV (lower figure). The intensities in the two channels are shown by the blue squares (I_B) and red circles (I_R), respectively.

The G_p value is thus a normalized range of values between 1 to -1 with smaller and negative values indicating deeper hydration of the bilayer and hence more fluid bilayers.

We measured the spectral shift of laurdan while translating a hot AuNP gradually closer to a GUV that was initially in the gel phase, as shown in the overlay in figure 2(C) (left panels). Initially the G_p values of the GUV are close to 0 (see figure 2(C), upper right) but as the AuNP approaches the left side of the GUV a clear shift can be detected towards lower G_p values on the left side of the GUV, see lower right panel in figure 2(C), thus verifying that the bilayer is indeed becoming more fluid. A quantification of the relative intensities within the intervals, I_B and I_R is shown in figure 2(D) as an average line scan (70 pixel lines) across the GUV before (upper panel) and after heating (lower panel). After local heating of the left side of the GUV a decrease is measured for the intensity in both channels but the decrease is more significant in the blue intensity channel, I_B , revealing that the bilayer has become more fluid.

2.2. Membrane pores exist in melting GUVs

Membranes undergoing a phase transition exhibit an anomalous high permeability which is thought to occur at the

interface between co-existing gel and fluid nanodomains in melting membranes. We investigated the nature of this permeability by locally melting GUVs, containing self-quenching concentrations of calcein dye, by using the experimental setup depicted in figure 1. When the gel phase GUVs were locally heated above the phase transition temperature, T_m , we measured transient and local efflux of the calcein which was detected as a local burst in intensity, see figure 3(A). The pores were transient as could be verified by quantifying the intensity over time at a fixed distance away from the GUV, see figure 3(B). The intensity in figure 3(B) shows an initial increase followed by decay in intensity, thus indicating that the pore has closed. By comparing data, as shown in figure 3(B), with the expected concentration of molecules predicted from Fick's second law of diffusion for an instantaneous point source, we have previously shown that the pore lifetimes of these events were on the order of 100 ms [4].

2.3. Pulling membrane tubes from melted regions

Pulling of membrane tubes from GUVs has been previously used for studying effects related to membrane curvatures. Membrane tubes are readily formed from fluid phase GUVs and together with micropipette aspiration for regulating the

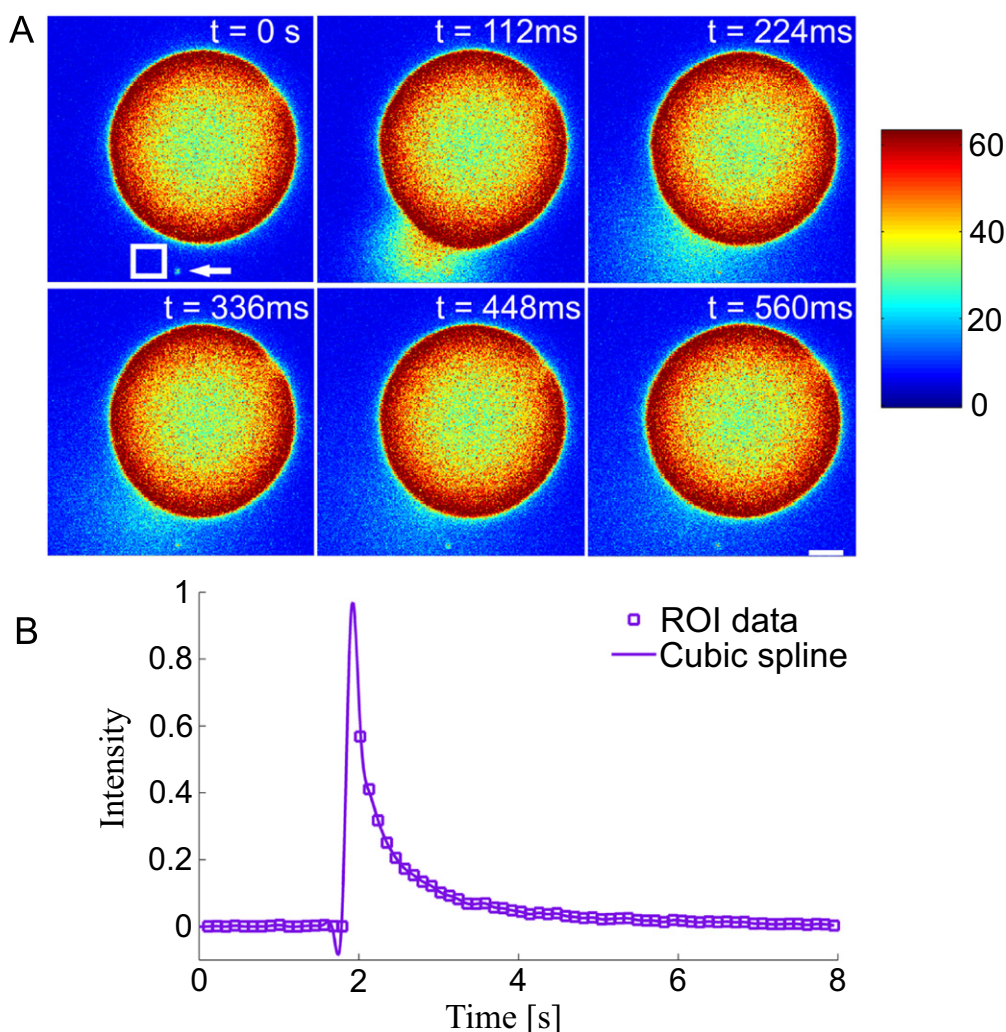


Figure 3. Transient and local permeability detected in a locally melted GUV. (A) Image sequence showing the dilution and de-quenching of calcein due to a local pore formation in the GUV membrane. The location of the optically trapped gold nanoparticle is indicated in the first image by a white arrow. Scale bar is $5 \mu\text{m}$. (B) The intensity is quantified within a ROI positioned $5 \mu\text{m}$ away from the transient pore on the GUV. The position of the ROI and AuNP is indicated by the square and arrow, respectively, in the first image of figure 3(A). The single peak indicates a single and transient pore formation in the GUV membrane.

membrane tension it is possible to obtain tubes with a spectrum of curvatures on which curvature sensing of protein binding can be investigated [16]. However, due to the rigidity of the gel phase it has not, until now, been possible to extract tubes from gel phase GUVs. The force needed to hold a membrane tube is given by [2]

$$f = 2\pi\sqrt{2\sigma\kappa}, \quad (2)$$

where σ is the membrane tension and κ is the bending rigidity of the membrane. κ has been measured for gel phase bilayers to be $57 K_B T$ (K_B is the Boltzmann's constant) for DPPC bilayers [17] whereas σ depends on osmotic pressure and the relative expansion of the bilayer due to aspiration or surface adhesion. According to equation (2) the force at a tension of e.g., $\sigma = 0.02 \text{ mN m}^{-1}$, will be $\sim 19 \text{ pN}$, however it is well known that tube formation also involves a barrier for formation which scales with the size of the adhesion patch between the particle and the membrane [21]. This barrier can

easily reach tens of pN for fluid phase GUVs and for gel phase GUVs this barrier can be higher than what optical tweezers typically can deliver ($f_{\text{max}} \sim 200 \text{ pN}$).

We therefore pulled membrane nanotubes from the fluid part of GUVs that were locally melted using a hot AuNP as shown schematically in figure 4(A). By combining optical heating (figure 4(B)) with optical pulling we could locally melt a GUV using an optically trapped AuNP and subsequently use a second trap to pull a membrane nanotube using a $4.95 \mu\text{m}$ polystyrene bead as shown in figure 4(A). The polystyrene bead was conjugated with streptavidin and the GUV contained a low fraction of biotinylated lipids to facilitate specific binding. The melted region was visualized by di-4-ANEPPDHQ (see figure 4(C)) and the nanotube was extruded from this region to a length exceeding $10 \mu\text{m}$. In figure 4(D) we also used Texas Red DHPE (TR-DHPE) to show a more uniform labeling of the GUV and tube membrane. Although TR-DHPE has a preference for fluid regions

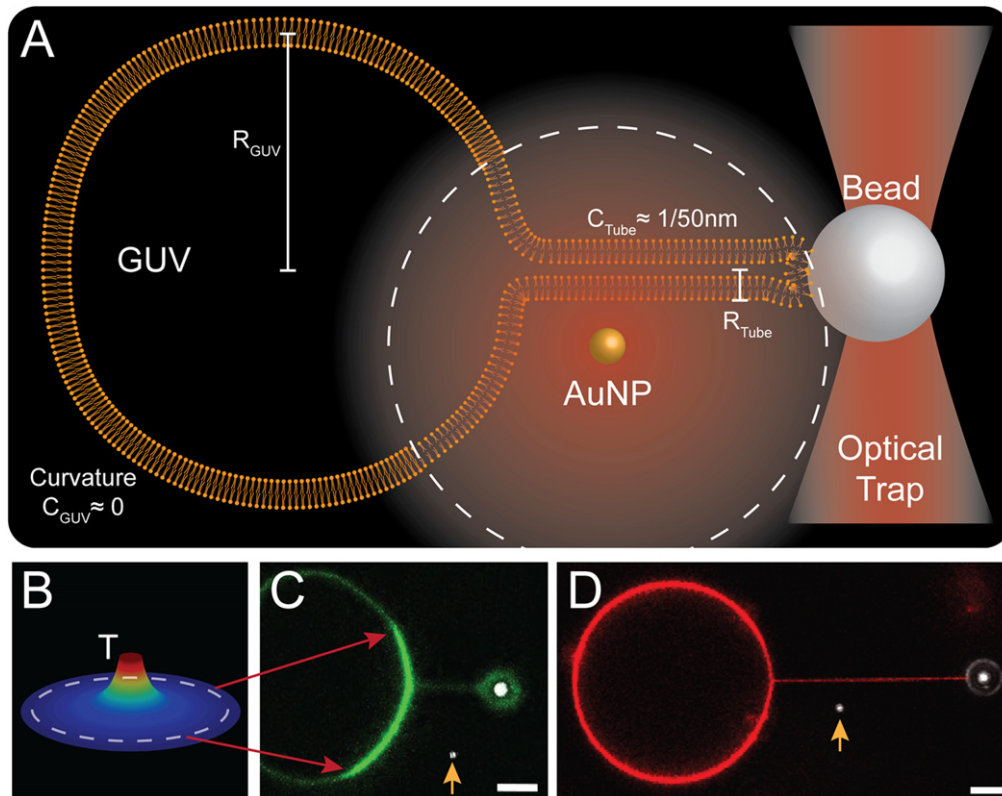


Figure 4. Tube pulling from local fluid regions within gel phase GUVs allows for studying membrane curvature effects on phase transitions. (A) Schematic diagram of tube pulling. An optically trapped AuNP is used to generate a fluid phase on the GUV and subsequently another trap holding a $d = 4.95 \mu\text{m}$ streptavidin coated polystyrene bead is used to pull out a membrane tether with $d \sim 100 \text{ nm}$ and thus with a curvature of $C \sim 1/50 \text{ nm}^{-1}$. The curvature of the GUV was typically three orders of magnitude lower, thus $C \sim 0 \text{ nm}^{-1}$. (B) The profile of the heating zone generated by the irradiated AuNP. The dashed circle in (A) and (B) marks the distance from the AuNP where the temperature equals the phase transition temperature, $T_m = 33 \text{ }^\circ\text{C}$ of the lipids. (C) Membrane tether and fluid region are imaged using di-4-ANEPPDHQ. The arrow indicates the location of the optically trapped AuNP. Scale bar is $5 \mu\text{m}$. (D) Imaging of the membrane tether and GUV system using the Texas Red DHPE lipid dye. The yellow arrow indicates the location of the optically trapped AuNP. The tube could be extended such that the temperature at the tip region was below T_m , indicating that curvature affects the melting point of the tether. Scale bar is $5 \mu\text{m}$.

it does not exhibit lateral partitioning on short time scales since the fluorophore exhibits very low mobility in the gel phase.

During nanotube extrusion we measure a uniform tube radius along the whole tube strongly indicating that the whole tube is in the same phase. Tube radius, R , membrane bending rigidity, κ , and membrane tension, σ , are related by

$$R = \sqrt{\frac{\kappa}{2\sigma}}. \quad (3)$$

Since membranes are significantly stiffer in gel phase than in fluid phase we would expect that co-existing phases on the tube would have different radii. However, as shown in figure 4(D), the tube radius stays relatively constant even though the end of the tube reaches a distance where the temperature is lower than the phase transition temperature. Occasionally, when long tubes are pulled we observe fission events which might be due to the onset of a tubular transition. Future studies will show if an actual phase boundary induced by a temperature gradient can be established on a tube made from DC₁₅PC without fissioning of the tube.

The effect of curvature on membrane phase transitions has been shown in bulk to result in lower melting

temperatures for highly curved bilayers [18]. The lower melting transition can be rationalized in terms of outer leaflet lateral stress upon significant bending of the membrane. Future experiments will address the effect of curvature on the transition temperature for membrane tubes and our aim is to explore the effect of inducing local transitions which could, as mentioned above, well lead to fission of the tube due to the discontinuities between the elastic constants between the two co-existing phases [19].

2.4. Thermal regulation of tube diameter

In traditional GUV/tube experiments the nanoscale diameter is regulated by controlling the membrane tension through an aspiration pipette [16]. However, temperature can also be employed for changing the tube diameter simply by regulating the laser power of the optical trap holding the gold nanoparticle, see figure 5(A). Initially, a substantial part of the GUV is melted by the heated gold nanoparticle (first image in figure 5(A)) and by successively decreasing the laser power, and hence the heating, we measure a decrease in the tube intensity (figure 5(B)) which is linearly related to the tube diameter. We note that the dye used in the experiment in

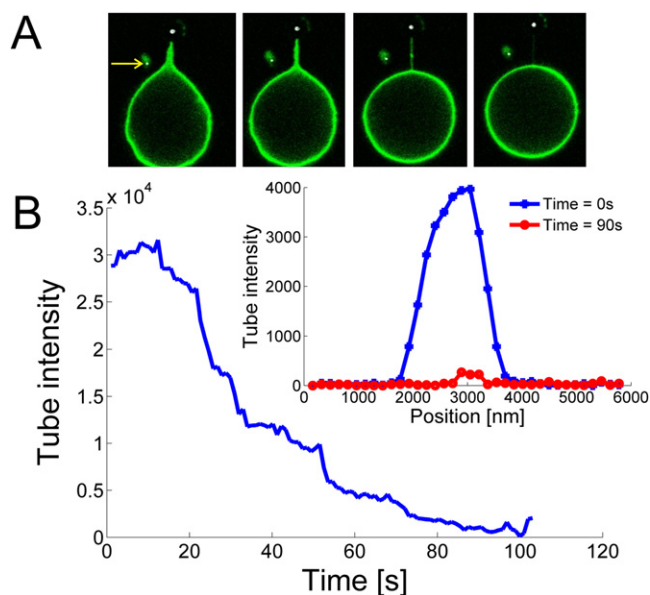


Figure 5. Variation of tube diameter with temperature. (A) Optical trapping of a gold nanoparticle (arrow) at decreasing laser powers results in a decrease in the tube intensity which is proportional to the tube diameter. See also supplementary movie 1. The GUV is labeled with TR-DHPE which does not partition notably between phases for this lipid mixture. (B) Quantification of the intensity as a function of time. The steps which are barely detectable in the curve correspond to sudden changes in laser power. Inset, intensity profile across the lipid tube, at $t=0$ s (blue curve) and at $t=90$ s (red curve).

figure 5 (TR-DHPE) does not partition between the gel and fluid phase on the time scale of this experiment and therefore we can assume a linear dependence between intensity and tube radius. An intensity profile across the initial and final tube in the inset of figure 5(B) reveals a substantial decrease in tube diameter. When the laser power is sufficiently low we observe fission of the tube as shown in supplementary information movie 1, available at stacks.iop.org/NANO/25/505101/mmedia.

A change in tube diameter can be rationalized by looking at the dependence of the radius on the bending rigidity as given in equation (3). The bending rigidity in equation (3) has been shown to change orders of magnitudes with small temperature changes (<1 °C) close to the phase transition temperature of DC₁₄PC lipid bilayers [14]. Therefore, we also expect significant changes to the radius of the tube according to equation (3) for similar lipid bilayers made from DC₁₅PC. Near T_m the lipid bilayer becomes extremely soft and the tube becomes consequently thinner and eventually fissions due to high curvature stress. We also note that membrane tension regulates tube radius through equation (3) and that the membrane tension does increase during cooling of the GUV/tube system in figure 5 due to a significant shrinkage of membranes during the fluid-to-gel transition.

2.5. Nanoscale domains by local heating of tubes

We also show how local membrane transitions can be established on lipid tubes made from more complex mixtures of lipids. Ternary mixtures of cholesterol, DPPC and DOPC

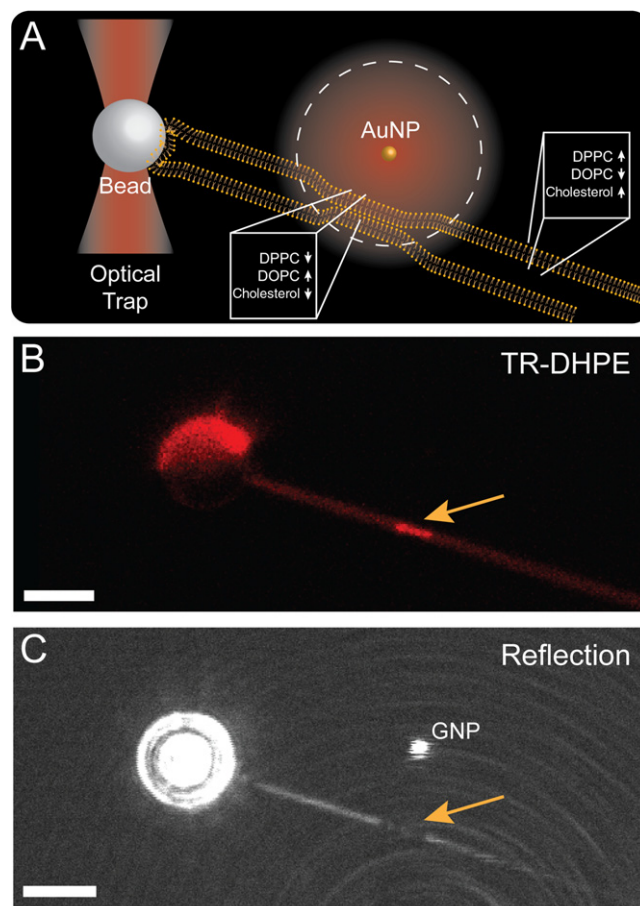


Figure 6. Local phase transition generated on a lipid tube pulled from a liquid ordered phase existing on a GUV made from DOPC, DPPC and cholesterol. (A) Schematic depiction of the experiment showing a local liquid disordered (l_d) phase being generated on a liquid ordered phase (l_o). The l_o phase is enriched in cholesterol whereas the l_d phase contains more unsaturated lipids (DOPC). (B) Local heating near a lipid tube results in transformation of the membrane from l_o phase to l_d phase (arrow) and a consequent enrichment of TR-DHPE in the nanoscale l_d phase. (C) Reflection image of the same tube as in (B). The black region corresponds to less reflection due to a smaller tube radius which is consistent with the fact that l_d phase has significantly lower bending rigidity than the l_o phase and hence forms thinner tubes according to equation (3). The bright spots are the trapped polystyrene particle and gold nanoparticle (GNP) respectively. Scale bars in (B) and (C) are $5 \mu\text{m}$.

can form GUVs containing two fluid phases with different order which are not as mechanically different as the gel and fluid phases presented in figure 4. In figure 6, a lipid tube is pulled from a GUV composed from a ternary mixture of DOPC, DPPC and cholesterol which contains co-existing phases of liquid ordered (l_o) and liquid disordered (l_d) phases labeled with TR-DHPE which partitions strongly into the (l_d) phase. A tube is pulled from the l_o phase and subsequent local heating of the tube reveals a melting transition on the tube. The increase in intensity in figure 6(B) results from the partitioning of TR-DHPE dye into the l_d phase but imaging of the tube in reflection mode [20] (figure 6(C)) reveals a dark region, with no detectable reflection light, which shows that the tube in fact becomes thinner at the region where local

melting occurs. This is consistent with the fact that the tube becomes fluid and hence attains a lower bending rigidity and consequently a smaller radius according to equation (3).

3. Conclusion

We have shown how local heating can be applied to investigate the physical properties of membranes. A locally induced membrane phase transition led to transient and local permeation of encapsulated calcein molecules which was detected as de-quenching of calcein as it left the interior of the GUV. The local phase change resulting from the heat gradient, established by the irradiated AuNP, was visualized by environmentally sensitive fluorophores that either selectively partition into the fluid phase or exhibit a spectral shift upon melting. Finally, this assay will allow further investigation of the interplay between curvature and phase transitions by performing local melting on lipid tubes pulled from GUVs being initially in an ordered phase.

4. Materials and methods

4.1. Sample preparation

GUVs were formed by using a standard electroformation device (Nanion Technologies, Germany). A lipid film was formed on an ITO coated glass slide and hydration was performed at $T=50\text{ }^{\circ}\text{C}$ which ensured that GUVs were formed above the phase transition temperature, $T_m=33\text{ }^{\circ}\text{C}$. The hydration solution contained either 600 mM sucrose (permeability experiments) or 300 mM sucrose (tube experiments). The GUVs were composed of 1,2-dipentadecanoyl-*sn*-glycero-3-phosphocholine (Avanti Polar Lipids, 850 350) and 0.3 mol% 1,2-dihexadecanoyl-*sn*-glycero-3-phosphoethanolamine, triethylammonium salt (Invitrogen, T1395MP, Texas Red DHPE) to label the vesicle membrane. Encapsulation of calcein within the GUVs was achieved by incubating 85 mM calcein (Invitrogen, C481) solution (adjusted to pH=7.2 using NaOH) with GUVs briefly at the phase transition temperature ($T_m=33\text{ }^{\circ}\text{C}$) or alternatively in the fridge at $5\text{ }^{\circ}\text{C}$ for >12 h. For imaging the fluid part of the GUV we used 1 mol% di-4-ANEPPDHQ (Invitrogen, D36802). The relative hydration level of the membrane was measured by including 0.5 mol% laurdan (Invitrogen, D250) in the lipid mixture. The three dyes were used in separate experiments and were pre-mixed with the lipids in chloroform. After the formation of the GUVs we noticed that the phase sensitive dye di-4-ANEPPDHQ does strongly partition into the solution when the GUVs were incubated below the phase transition temperature. However, after melting the GUV locally, the dye (which has a very low quantum yield in solution) strongly partitioned into the fluid phase of the GUV. In permeability experiments, the GUVs were allowed to settle on a clean glass coverslip, passivated with BSA or α -casein (Sigma Aldrich), in a solution that was iso-osmolar with the inside solute concentration (calcein, sucrose and NaOH). The remaining

dye was carefully diluted from the sample by pipetting. In the permeability experiments 300 mM NaCl was used to balance the osmotic pressure from the interior solution. AuNPs ($d=80\text{ nm}$) were purchased from British Biocell International (British Biocell International, BBI). Tubes were pulled by using streptavidin coated polystyrene beads, purchased from Bangs Laboratories, with a diameter of $4.95\text{ }\mu\text{m}$.

4.2. Experimental setup

The setup included a dual optical trapping system ($\lambda=1064\text{ nm}$, Spectra Physics J201-BL-106C) coupled into a confocal fluorescence microscope (Leica SP5) equipped with a water immersion objective (Leica, PL APO NA: 1.2, 63 \times) and a piezo electric stage for translating the sample (PI 731.20, Physik Instrumente, Germany). One of the laser traps could be controlled by a piezo mirror (Mad City Labs) allowing a trapped AuNP to be positioned near the GUV or near the membrane nanotube. In the permeability assay we continuously decreased the distance between the AuNP and the GUV at 100 nm s^{-1} . AuNPs were imaged using an argon laser line ($\lambda=514\text{ nm}$) and by collecting the backscattered light using an acousto optical beam splitter [20]. Excitation of calcein and di-4-ANEPPDHQ was performed at $\lambda=488\text{ nm}$ and TR-DHPE was excited at $\lambda=594\text{ nm}$. Fluorescent and scattered light was collected using photomultiplier tubes. Laurdan was excited at $\lambda=405\text{ nm}$ and the emission light was collected using a HyD detector installed on the SP5 Leica confocal system. Calcein plumes were recorded at 112 ms time resolution to capture the dynamics of the permeation events.

4.3. Data analysis

All data and image analysis was done in Matlab using the Image Processing Toolbox.

Acknowledgments

We acknowledge financial support from the University of Copenhagen, Excellence Program, the Lundbeck Foundation, and the Villum Kann Rasmussen Foundation.

References

- [1] Huang X *et al* 2006 Cancer cell imaging and photothermal therapy in the near-infrared region by using gold nanorods *J. Am. Chem. Soc.* **128** 2115–20
- [2] Huang H *et al* 2010 Remote control of ion channels and neurons through magnetic-field heating of nanoparticles *Nat. Nanotechnology* **5** 602–6
- [3] Bendix P M *et al* 2014 Optical trapping of nanoparticles and quantum dots *IEEE J. Sel. Top. Quantum Electron.* **20** 4800112
- [4] Andersen T, Kyrsting A and Bendix P M 2014 Local and transient permeation events are associated with local melting of giant liposomes *Soft Matter* **10** 4268–74

- [5] Kyrsting A *et al* 2011 Heat profiling of three-dimensionally optically trapped gold nanoparticles using vesicle cargo release *Nano Lett.* **11** 888–92
- [6] Bendix P M, Reihani S N and Oddershede L B 2010 Direct measurements of heating by electromagnetically trapped gold nanoparticles on supported lipid bilayers *ACS Nano* **4** 2256–62
- [7] Atia L and Givli S 2014 A theoretical study of biological membrane response to temperature gradients at the single-cell level *J. R. Soc. Interface* **11** 20131207
- [8] Mouritsen O G and Zuckermann M J 1985 Softening of lipid bilayers *Eur. Biophys. J.* **12** 75–86
- [9] Papahadjopoulos D *et al* 1973 Phase transitions in phospholipid vesicles. Fluorescence polarization and permeability measurements concerning the effect of temperature and cholesterol *Biochim. Biophys. Acta* **311** 330–48
- [10] Cisse I *et al* 2007 Fueling protein DNA interactions inside porous nanocontainers *Proc. Natl Acad. Sci. USA* **104** 12646–50
- [11] Blicher A *et al* 2009 The temperature dependence of lipid membrane permeability, its quantized nature, and the influence of anesthetics *Biophys. J.* **96** 4581–91
- [12] Antonov V F *et al* 2005 Soft perforation of planar bilayer lipid membranes of dipalmitoylphosphatidylcholine at the temperature of the phase transition from the liquid crystalline to the gel state *Eur. Biophys. J.* **34** 155–62
- [13] Jin L *et al* 2006 Characterization and application of a new optical probe for membrane lipid domains *Biophys. J.* **90** 2563–75
- [14] Dimova R, Pouligny B and Dietrich C 2000 Pretransitional effects in dimyristoylphosphatidylcholine vesicle membranes: optical dynamometry study *Biophys. J.* **79** 340–56
- [15] Sezgin E *et al* 2012 Elucidating membrane structure and protein behavior using giant plasma membrane vesicles *Nat. Protocols* **7** 1042–51
- [16] Ramesh P *et al* 2013 FBAR syndapin 1 recognizes and stabilizes highly curved tubular membranes in a concentration dependent manner *Sci. Rep.* **3** 1565
- [17] Picas L, Rico F and Scheuring S 2012 Direct measurement of the mechanical properties of lipid phases in supported bilayers *Biophys. J.* **102** L01–03
- [18] Nagano H *et al* 1995 Effect of vesicle size on the heat capacity anomaly at the gel to liquid-crystalline phase transition in unilamellar vesicles of dimyristoylphosphatidylcholine *Phys. Rev. E* **52** 4244–50
- [19] Allain J M *et al* 2004 Fission of a multiphase membrane tube *Phys. Rev. Lett.* **93** 158104
- [20] Bosanac L *et al* 2008 Efficient optical trapping and visualization of silver nanoparticles *Nano Lett.* **8** 1486–91
- [21] Kaster G, Cacciuto A, Derényi I, Frenkel D and Dogterom M 2005 Force barriers for membrane tube formation *Phys. Rev. Lett.* **94** 068101